



Concentrating solar thermal desalination: Performance limitation analysis and possible pathways for improvement

Yanjie Zheng^a, Rodrigo Caceres Gonzalez^d, Marta C. Hatzell^d, Kelsey B. Hatzell^{a,b,c,*}

^a Department of Mechanical Engineering, Vanderbilt University, Nashville, TN 37240, USA

^b Interdisciplinary Material Science Program, Vanderbilt University, Nashville, TN 37240, USA

^c Chemical and Biomolecular Engineering, Vanderbilt University, Nashville, TN 37240, USA

^d George W. Woodruff School of Mechanical Engineering, Georgia Institute of Technology, Atlanta, GA 30313, USA

ARTICLE INFO

Keywords:

Desalination
Concentrating Solar collector
Solar thermal desalination
Specific water production
Endo-reversible thermodynamics

ABSTRACT

Solar thermal desalination is a viable approach for sustainable water production. Current thermal desalination technologies suffer from high specific energy consumption and energy mismatch. Concentrating solar collectors operate with high temperature energy and desalination systems operate with low temperature energy which leads to large exergy destruction. Herein, a thermodynamic model of an ideal concentrating solar-distillation process is developed to evaluate system integration and performance limitations (specific water production). Three different heating architectures are examined to understand how solar collector absorber temperature, concentration ratio, and recovery ratio impact system performance. A reversible solar distillation system operating with a concentration ratio of 10 at the optimal absorber temperature of 507 K can achieve a maximum specific water production of $\sim 166.3 \text{ g s}^{-1} \text{ m}^{-2}$ as the recovery ratio (rr) approaches zero. An endo-reversible heat engine model was formulated to consider system irreversibilities. Systems with irreversibilities ($R = 0.001 \text{ K/kW}$ or 0.005 K/kW) experience a decrease in the water production rate to $8.8 \text{ g s}^{-1} \text{ m}^{-2}$ ($rr = 51.4\%$) and $1.9 \text{ g s}^{-1} \text{ m}^{-2}$ ($rr = 65.2\%$). For efficient integration of solar collectors with thermal desalination systems, it is critical to adopt appropriate heating configurations and control absorber temperatures, system recovery ratio, and system irreversibilities.

1. Introduction

Solar thermal desalination technologies may be a viable approach toward addressing growing water shortages in geographical areas with abundant solar resources [1–5]. However, wide-scale implementation of solar thermal desalination faces both thermodynamic and economic barriers [6–11]. Irreversibilities in the energy recovery system prevent complete recovery of latent heat during the desalination step, which results in enormous exergy destruction [12–15]. Thus, thermal desalination systems suffer from low second law efficiencies ($<10\%$) when compared to reverse osmosis ($\sim 30\%$) [12,16]. Inadequate exergy utilization leads to higher specific energy consumption and leveled cost of water when compared with pressure-driven desalination approaches. As a result, thermal desalination plants produce $\sim 26\%$ less water than reverse osmosis worldwide [17].

Conventional thermal desalination plants operate at low temperatures due to saturation and fouling temperature limitations [18,2,4].

Coupling solar technologies directly with a thermal desalination system will lead to large exergy losses due to the mismatch in energy quality supplied (e.g., high temperature solar) and the energy quality required (e.g., low-temperature desalination). Several different system integration strategies have been envisioned to overcome this inherent challenge. Hybrid concentrated solar power (CSP) based cogeneration systems that produce both electricity (power) and waste heat (desalination) are one possible pathway to avoid large exergy losses associated with thermal desalination systems [19–24]. However, the water production capacity and rate is limited by the subsequent scale and economics of the power cycle. CSP-desalination cogeneration approaches have the benefit of working with thermal (waste heat) and pressure-driven (electricity) desalination approaches [5]. Thus, there is a significant body of work examining various power cycles (Organic Rankine, CO_2 supercritical, Brayton, etc.) [25–32] that may be suitable for the production of both power and freshwater.

Regardless of the cogeneration approach, efficient energy transfer

* Corresponding author at: Department of Mechanical Engineering, Vanderbilt University, Nashville, TN 37240, USA.

E-mail address: kelsey.b.hatzell@vanderbilt.edu (K.B. Hatzell).

from a high temperature concentrating solar collector to a low-temperature desalination system represents a significant challenge and is paramount in order to decrease the levelized cost of water. However, most studies to date focus either on improving the individual performance of the power component (CSP) or the water device (desalination). The latter approach has led to strategies to achieve solar-to-power and energy-to-water. Numerous studies have employed ideal and finite-time thermodynamic (endo-reversible heat engine) models to evaluate the performance properties of a concentrated solar power (CSP) plant and these analyses reveal the intrinsic trade-off between solar collector ambient heat loss and power generation efficiency [33–39]. Optimization of key variables (absorber operating temperatures and concentration ratio) are necessary for high performing CSP plants. From the perspective of desalination processes, combining first and second laws of thermodynamics can obtain the minimum energy consumption for separation (e.g. desalination) [40]. An ideal thermal separation process is analogous to a Carnot heat engine where water production operating temperature is thermodynamically limited to the boiling point of the solution [41]. Traditional finite-time thermodynamic analyses used for heat engine analysis does not consider flow work in the desalination subsystem or irreversibilities in the waste heat recovery. Thus, finite-time thermodynamic analyses are unreliable in evaluating the performance of these combined systems [42,43] and there is a need for more rigorous models of combined power and desalination systems (solar-to-power and -water) which can be optimized for performance and simultaneously capture irreversibilities associated with hybrid treatment trains.

This paper proposes a thermodynamic model for a thermal desalination process coupled with three different solar collector heating configurations (i.e., direct, cascading, and lumped) to study the performance limitation. The work accounts for irreversibilities via introducing an endo-reversible engine model and evaluates how system properties such as thermal resistance (irreversibilities), evaporator temperature, feedwater salinity, and recovery ratio impact the overall performance. Careful analysis and comparison of the reversible and irreversible scenarios provides critical insight into optimal design of

solar-thermal desalination systems. Hybrid treatment trains represent a potential pathway toward increasing the energy efficiency of solar-desalination plants but it will require systems with exquisite control over absorber temperature, system-level recovery ratio, and heating architectures.

2. System description

Herein, three different energy transfer architectures are evaluated to understand design and performance trade-offs for a generic solar-thermal desalination system. Thermodynamics is integrated into the analysis with an ideal solar thermal desalination model modified with an ideal distillation process model (Supporting Information S1) [40]. Both ideal and non-ideal scenarios for energy transfer and recovery are systematically evaluated [44,14,45]. The optimal case (Carnot) is directly compared to an endo-reversible system architecture to examine the impact of irreversibilities on system performance (Section 3.2).

2.1. Distillation process driven by solar collectors

An idealized solar distillation process for water desalination was modeled to evaluate system thermodynamics (Fig. 1). The model is composed of an evaporator that vaporizes incoming saline water, a condenser, and a heat exchanger for energy recovery. Waste heat from the effluent brine stream (\dot{m}_b) and pure water (\dot{m}_p) is used to preheat (T_L) the incoming saline water (\dot{m}_s) in the heat exchanger. Subsequently, the saline water temperature is brought to a boiling temperature in heater 1 (H1). The saline water absorbs heat isothermally in the evaporator, which produces an effluent stream of superheated water vapor with a mass flow rate (\dot{m}_p) at chiller 3 (C3). The superheated vapor undergoes a phase change (saturated water vapor, T_C) in the chiller and is further condensed to a saturated liquid phase in the condenser.

The model contains numerous Carnot-type heat engines (E) and heat pumps (HP) in order to evaluate the minimum work required for

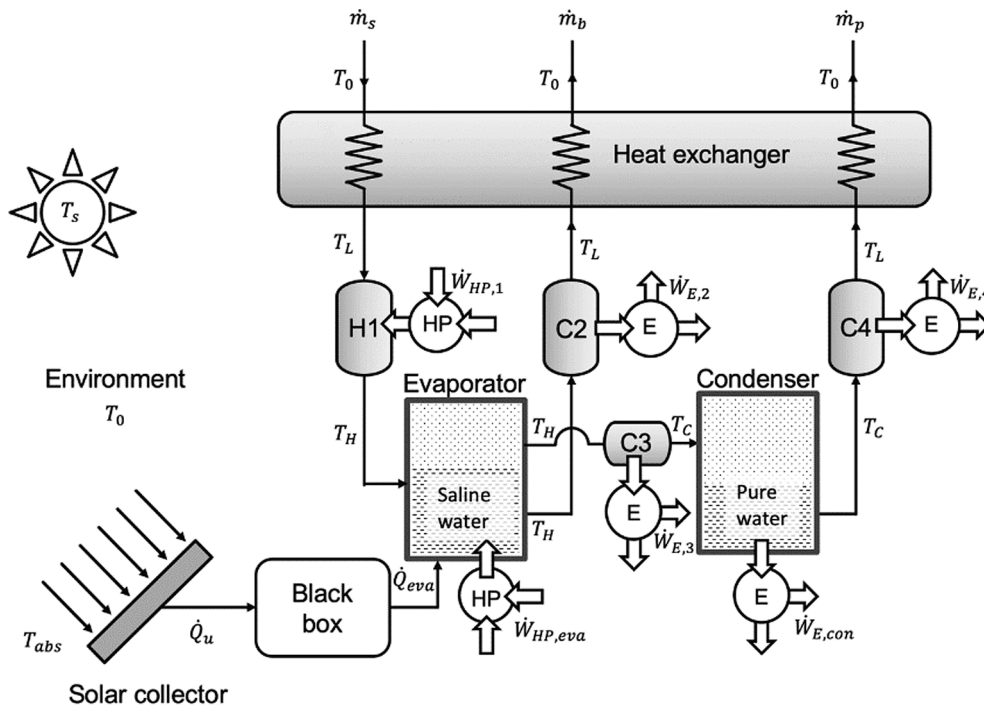


Fig. 1. Schematic diagram of an ideal solar distillation model. Heaters (H), heat pumps (HP), heat engines (E) and chillers (C2/C4) can be implemented to model solar desalination.

separations. Heat rejected is directly converted to useful work in heat engines (\dot{W}_E), and heat addition is driven by heat pumps (\dot{W}_{HP}). The heat exchanger is assumed to be infinitely large and 100% efficient under reversible assumptions and finite under the irreversible assumption. This assumption ensures that there is no exergy destruction in the heat exchanger during reversible operating conditions. A finite heat exchanger area (irreversible) will result in finite temperature differences between hot and cold fluid streams that will affect the system's overall performance when the energy losses outside the heat exchanger cannot be fully recovered (Section 3.2).

Actual desalination systems with energy recovery, will preheat the feedwater with the effluent produced freshwater. Herein, Carnot heat engines and Carnot heat pumps are used to model an ideal heat recovery process. Thermal energy is introduced into the system via solar collectors. The solar collectors are directly connected to an evaporator with a black box. The black box represents a variety of different energy transfer devices (heating configurations) (Fig. 2a-c). The role operating conditions and energy recovery architectures impact system performance are evaluated using the combined model.

2.2. Solar collector heating configurations

Solar thermal desalination systems are often characterized as indirect or direct [46]. Systems that are direct have a single system where evaporation and condensation occurs. Indirect solar thermal desalination systems consist of two separate subsystems (solar collector and desalination unit). Indirect techniques are favored to achieve desalination at scale, and direct thermal desalination techniques are practical in distributed applications. Herein, we consider an indirect thermal desalination which contains a solar collector unit in tandem with a desalination plant. Three different energy transfer architectures are explored for transferring heat between the solar collectors and evaporator (Fig. 2a-c). The best architecture will deliver the largest quantity of heat transfer to the evaporator (\dot{Q}_{eva}) at a fixed temperature. Understanding the trade-offs between system architecture and operating performance (i.e., specific water production) is essential for improving the performance of existing solar desalination technologies and engineering next-generation systems.

Heating configuration **a** (Fig. 2a) directly transfers heat from the solar collector to the evaporator without any intermediate engineering devices. Conventional indirect solar thermal desalination technologies (e.g., solar multi-stage flash and solar multi-effect distillation) often utilize this heating strategy [13,47,48]. Direct heating strategies are very common because they do not require the need for any additional devices. However, direct heating methods typically suffer from high exergy destruction because of the mismatch in energy quality between the source (solar collector) and the sink (distillation system). Concentrating technologies such as a compound parabolic concentrator, linear Fresnel reflector, and parabolic through concentrator can provide thermal energy ≥ 200 °C [49]. The source temperature of a solar tower system with a heliostat field can achieve 500–2000 °C. These operating conditions are incompatible with most thermal desalination technologies that operate at much lower temperatures. Thermal desalination systems operate at low temperatures to avoid scaling and saturation temperature limitation (e.g., the top brine temperatures of multi-stage flash and multi-effect distillation is less than 110 °C and 70 °C) [50]. To overcome these challenges, most thermal desalination plants employ low-concentrating or non-concentrating solar systems (e.g., flat plate collectors).

To take advantage of the elevated operating temperatures, we consider two additional energy transfer architectures (**b** and **c**). System **b** and **c** (Fig. 2b and c) employ Carnot heat engines to generate work in order to drive a Carnot heat pump. The Carnot heat pump transforms low-grade heat from the environment into a usable source for the desalination system [51]. Architecture **b** transfers less work to the heat

pump, but provides more direct heat transfer between the heat engine and the evaporator. In contrast, heating architecture **c** releases heat to the environment and transfers more work to the Carnot heat pump. These two heating architectures (Fig. 2b and c) are relevant to existing applications and may enable future high temperature operating regimes. The consumption of heat can be directly converted into exergy (in terms of electrical or mechanical work) with the Carnot efficiency with reversible assumption. Therefore, the concentrated solar power (CSP) cogeneration plant is an irreversible form of architecture **b** since the solar collector releases heat to thermal desalination units through a power cycle. The structure of the solar organic Rankine cycle-reverse osmosis system is similar to architecture **c** since the solar collector runs the power cycle and rejects heat to the environment for driving the membrane system.

3. Mathematical modeling

A mathematical model of a distillation process driven by solar collectors under ideal (i.e., reversible) and irreversible conditions was built. Herein, we use specific water production (SWP), which represents the water production rate (\dot{m}_p) per unit area of the solar collector (A_c), to evaluate the performance of solar desalination system.

$$SWP = \frac{\dot{m}_p}{A_c} = \frac{\dot{Q}_{max}/A_c}{q_{sep,min}} \quad (1)$$

where the area of the solar collector is the production of the absorber area (A) and the concentration ratio (C) [52], which is dependent on solar collectors geometry (conical, parabolic, spherical) [53,54].

$$A_c = C \cdot A \quad (2)$$

The solar desalination system performs optimally when the heat transfer rate from the solar collector system is maximized (\dot{Q}_{max}), and the separation heat per unit mass of pure water production is minimized ($q_{sep,min}$).

3.1. Ideal condition

3.1.1. Solar collector system and heating strategies

Three different solar heating configurations are considered (Fig. 2). The heat transfer from the solar collector to the evaporator is related to the absorber temperature of the solar collector (T_{abs}), the evaporator operating temperature (T_H), and the ambient environment (T_0). For effective operation, $T_{abs} \geq T_H > T_0$. Assuming reversible heat pumps and engines, the amount of heat transfer to the evaporator for each configuration are:

$$\dot{Q}_{eva,a} = \dot{Q}_u \quad (3a)$$

$$\dot{Q}_{eva,b} = \dot{Q}_1 + \dot{Q}_2 = \dot{Q}_u \left[\frac{T_H}{T_{abs}} + \left(1 - \frac{T_H}{T_{abs}} \right) \frac{T_H}{T_H - T_0} \right] \quad (3b)$$

$$\dot{Q}_{eva,c} = \dot{Q}_3 = \dot{Q}_u \left(1 - \frac{T_0}{T_{abs}} \right) \frac{T_H}{T_H - T_0} \quad (3c)$$

Eq. (3b) can be reduced to Eq. (3c) for a reversible system.

The three heating configurations provide the same amount of heat when the solar collector absorber temperature equals to the evaporator temperature. Otherwise when the surface temperature of the solar collector (T_{abs}) exceeds the evaporator temperature (T_H), the heat supply for architecture **b** and **c** will be greater than **a**. Architecture **a** suffers from exergy loss due to finite temperature differences during heat transfer. Furthermore, architecture **b** and **c** can collect a higher quality of energy at higher solar collector absorber temperatures (T_{abs}) and fully recover it through Carnot heat pumps at lower evaporator temperature. No exergy destruction results in a greater heat transfer to the evaporator

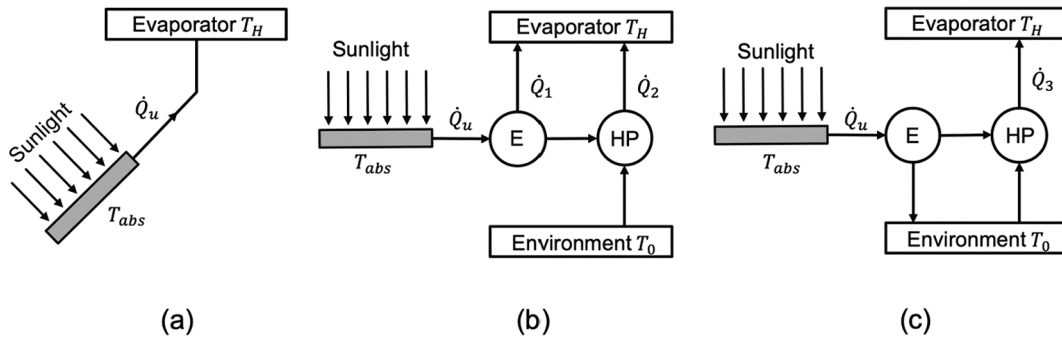


Fig. 2. Schematic diagrams of three different solar collector heating configurations. Direct (a) and indirect (b,c) heating strategies can be implemented with a variety of desalination approaches.

in both cases. However, higher absorber temperature (T_{abs}) will reduce the heat collected by the solar collector (\dot{Q}_u) due to greater heat loss from the surface through convection and radiation.

$$\dot{Q}_u = A\tau\alpha [CI_s + (1 - C \cdot F)\sigma T_0^4 - \sigma T_{abs}^4] - AU_L(T_{abs} - T_0) \quad (4)$$

In Eq. (4) [13,33], A is the area of the solar collector absorber (i.e., receiver), τ is the transmissivity of the glass surface on top of the solar collector, and α is the absorptivity, which would be less than 1 when the solar collector receiving surface is assumed to be an incomplete black body. C is the concentrating ratio of the collector system, and I_s is the solar irradiance rate per unit area. The view factor of the collector to the sun is $F \approx 2.16 \times 10^{-5}$ and the Stefan–Boltzmann constant is $\sigma = 5.67 \times 10^{-8} \text{W}/(\text{m}^2 \cdot \text{K}^4)$. The total convection and conduction loss coefficient from the receiver is denoted by U_L .

For a well-insulated solar collector, convection and conduction heat loss is smaller than radiation heat loss. The heat loss by conduction and convection will be zero for an ideal solar collector ($\tau = 1, \alpha = 1$) and Eq. (4) can be simplified to:

$$\dot{Q}_u = A [CI_s + (1 - C \cdot F)\sigma T_0^4 - \sigma T_{abs}^4] \quad (5)$$

Thus, the maximum heat transfer rate to the desalination system can be derived by substituting Eq. (5) into Eq. (3):

$$\dot{Q}_{eva} = A [CI_s + (1 - C \cdot F)\sigma T_0^4 - \sigma T_{abs}^4] \left(1 - \frac{T_0}{T_{abs}}\right) \frac{T_H}{T_H - T_0} \quad (6)$$

It is possible to find and validate the optimal absorber temperature ($T_{abs,opt}$) that enables the maximum heat supply to the desalination system (\dot{Q}_{max}) by taking the first and second derivatives of Eq. (6). The maximum specific water production of solar desalination system can be calculated by combining Eq. (1), Eq. (2), and Eq. (6).

3.1.2. Distillation system

The minimum work of separation for the desalination process is the Gibbs free energy difference between the inlet and outlet fluids[55,56].

$$\dot{W}_{sep,min} = \dot{m}_p g_p + \dot{m}_b g_b - \dot{m}_s g_s \quad (7)$$

where, g represents the specific Gibbs free energy and \dot{m} is the mass flow rate. The subscripts $p, s,$ and b denotes the produced pure water, the influent saline water, and the effluent concentrated brine. According to the definition of recovery ratio ($rr = \frac{\dot{m}_p}{\dot{m}_s}$) and the mass balance equation ($\dot{m}_s = \dot{m}_p + \dot{m}_b$), the minimum work of separation for unit mass of produced water ($w_{sep,min} = \frac{W_{sep,min}}{\dot{m}_p}$) can be expressed by:

$$w_{sep,min} = (g_p - g_b) - \frac{1}{rr} (g_s - g_b) \quad (8)$$

For the heat-driven desalination (i.e., distillation process), the minimum heat of separation is relevant to the Carnot efficiency under its operating temperature (T_H)[12,57]:

$$q_{sep,min} = \frac{w_{sep,min}}{1 - \frac{T_0}{T_H}} = \frac{(g_p - g_b) - \frac{1}{rr} (g_s - g_b)}{1 - \frac{T_0}{T_H}} \quad (9)$$

The specific Gibbs free energy is dependent on thermophysical properties of the fluid and is related to the fluid properties like temperature, salinity and pressure [58–61]. The temperature (T_0) and pressure (P_0) are taken as environmental conditions. When the salinity of inlet saline water (y_s) and recovery ratio (rr) are given, salinity (y_b) of brine water can be calculated by:

$$y_b = \frac{y_s - rr \cdot y_p}{1 - rr} \quad (10)$$

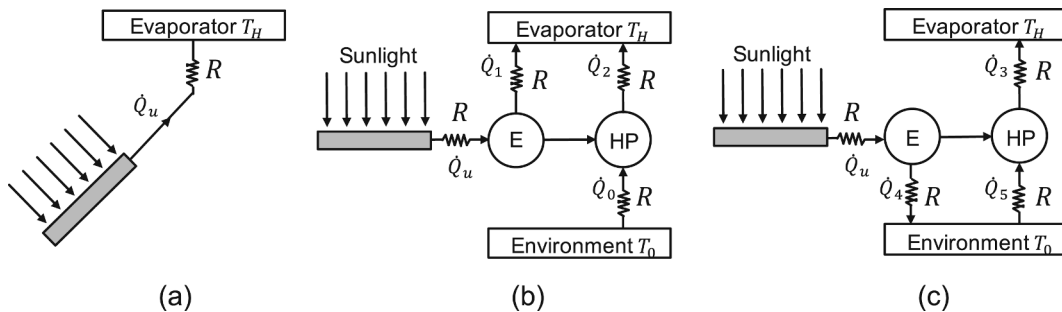


Fig. 3. Schematic diagrams of three different solar collector heating configurations considering irreversibilities. Direct heating strategies (a) and indirect heating strategies (b,c) can be used to transfer energy from the solar collector to desalination unit. E = Heat engine, HP = Heat Pump, Q = Heat Transfer, and R = resistances or irreversibility.

To simplify the equations, we assume salinity of the product water is pure water (i.e., $y_p = 0$), then

$$y_b = \frac{y_s}{1 - r_f} \quad (11)$$

Some distillation systems operate below ambient pressure to avoid scaling at high temperatures and to reduce the impact of non-condensable gasses on mass transfer resistances [13]. Operating below ambient pressure may require additional flow work to move the pure and brine water out of the system. Assuming that the feedwater is incompressible, the flow work per unit mass of pure water (w_f) is:

$$w_f = -\frac{1}{r_f} v_s (P_0 - P) (1 - r_f) \quad (12)$$

where v_{sw} is the specific volume of the saline water, and r_f is the recovery rate of the flow work done by the fluid at the inlet due to the pressure difference. If $r_f = 100\%$, the impact of flow work can be neglected. We assume the distillation operating pressure (P) is the saturated pressure [58,62] of the feed saline water corresponding to the evaporator temperature (T_H). Thus, the total separation work required to produce a unit of pure water ($w_{sep,tot}$) is:

$$w_{sep,tot} = w_{sep,min} + w_f \quad (13)$$

Combining Eq. (13) with Eq. (9) and Eq. (1) results in a relationship for the maximum specific water production which includes energy associated with flow work.

3.2. Irreversible condition

The above analysis assumes the system operates reversibly. However, irreversibilities in the system (such as thermal resistance, heat loss, finite temperature heat transfer, and friction) will create operating scenarios where the efficiency falls below the Carnot limit. It can be challenging to quantify the effects of system irreversibilities. Therefore, this paper applies an endo-reversible heat engine model [63,64,33] to account for any irreversibilities. The model assumes all irreversibilities exist in the form of thermal resistance outside of the Carnot heat engine and Carnot heat pump (Fig. 3). Therefore, the Carnot efficiency calculation is still valid for the heat engine. However, the thermal resistance will cause the reservoir temperature to decrease or increase for a specified temperature differential (ΔT). Thus, the Carnot heat engine will operate in a narrower temperature range, thereby lower efficiency. The

Carnot heat pump requires more work input to operate on a broader temperature range and causes a reduction in the coefficient of performance. In general, different heat engines and heat pumps, as well as their heat exchange with reservoirs, should have different thermal resistance. To simplify the calculation, we assume that the area (A_c) and the heat transfer coefficient (U) of the heat exchange surfaces are equal. Thus, all thermal resistances $R = \frac{1}{UA_c}$ (K/kW) are the same. Future research can adjust the value of each thermal resistance for analysis of different situations. The temperature difference (ΔT) due to irreversibilities can be calculated directly from the heat exchange amount \dot{Q} .

$$\Delta T = \dot{Q} \cdot R \quad (14)$$

3.2.1. Solar heating architectures

We quantify the maximum energy transfer to the desalination system under irreversible scenarios for three different heating configurations, respectively (Fig. 3). Since Eq. (6) has taken heat loss of solar collectors into account, the following analysis will not consider the additional impact of solar collector irreversibility.

There is no heat engine or heat pump in the direct heating architecture **a** (Fig. 3a). However, the thermal resistance between the solar collector and the evaporator could degrade the quality of the transferred energy. The thermal resistance has an impact on the optimal surface temperature of the solar collectors, thereby affecting the maximum heat supply. The smaller the absorber temperature of the solar collector, the less heat loss from the surface and exergy loss due to temperature difference heat transfer. Therefore, in an irreversible condition, the optimal absorber temperature ($T_{abs,opt}$) enables the maximum solar collector's heat supply ($\dot{Q}_{eva,a,irr} = \dot{Q}_u$) when the thermal energy transfer to the evaporator isothermally after quality degradation at the thermal resistance. Combining Eq. (5) with Eq. (15) can solve the optimal absorber temperature ($T_{abs,opt}$).

$$T_{abs,opt} - T_H = \dot{Q}_u \cdot R \quad (15)$$

For heating architecture **b** (Fig. 3b), according to Eq. (6), the optimal operating temperature of the system in the reversible state is a trade-off between providing higher exergy and suffering more heat loss. However, under irreversible conditions, the performance reduction of the heat engine and heat pump decreases the exergy efficiency. Therefore, the optimal absorber temperature deviates from the results of ideal conditions. Solving the following equations and Eq. (5) can find the relationship between heat supply to the evaporator (\dot{Q}_1 and \dot{Q}_2) and receiver surface temperature (T_{abs}) under thermal resistance of R .

$$\frac{\dot{Q}_1}{\dot{Q}_u} = \frac{T_H + \dot{Q}_1 \cdot R}{T_{abs} - \dot{Q}_u \cdot R} \quad (16)$$

$$\dot{Q}_u - \dot{Q}_1 = \dot{Q}_2 - \dot{Q}_0 \quad (17)$$

$$\frac{\dot{Q}_2}{\dot{Q}_0} = \frac{T_H + \dot{Q}_2 \cdot R}{T_0 - \dot{Q}_0 \cdot R} \quad (18)$$

The optimal absorber temperature ($T_{abs,opt}$) for the maximum heat supply ($\dot{Q}_{eva,b,irr}$) should make the first derivative equation of Eq. (19) equal to 0, and the secondary derivative equation less than 0.

$$\dot{Q}_{eva,b,irr} = \dot{Q}_1 + \dot{Q}_2 \quad (19)$$

Similarly, we can find the maximum heat supply of architecture **c** under irreversible condition by solving the following equations and taking the first and the second derivative of $\dot{Q}_3 = \dot{Q}_{eva,c,irr}$ with respect to the absorber temperature (T_{abs}).

$$\frac{\dot{Q}_4}{\dot{Q}_u} = \frac{T_0 + \dot{Q}_4 \cdot R}{T_{abs} - \dot{Q}_u \cdot R} \quad (20)$$

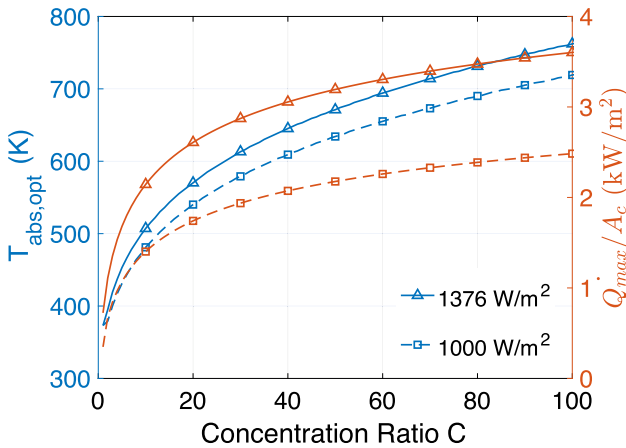


Fig. 4. The optimal absorber temperature ($T_{abs,opt}$) and maximum normalized heat supply to the desalination system (\dot{Q}_{max}/A_c) increases with concentration ratio (C) with a decreasing growth rate.

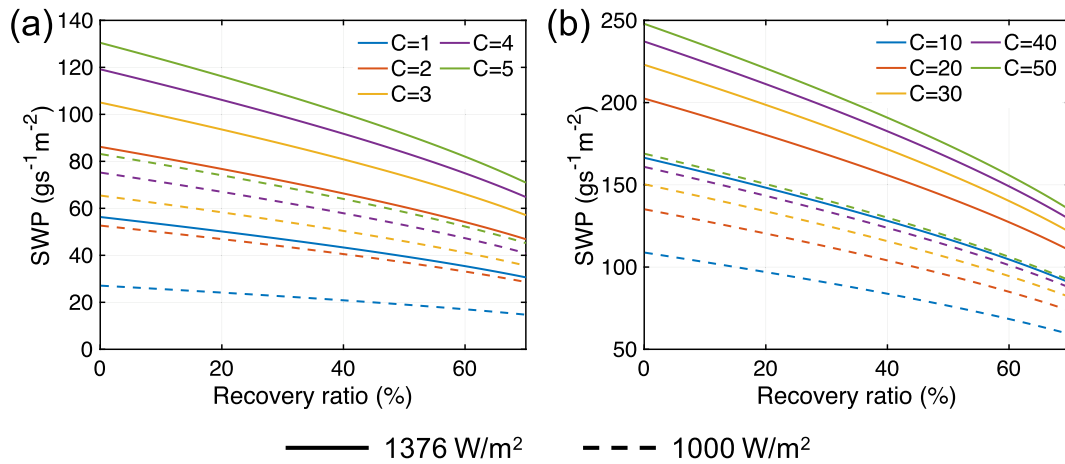


Fig. 5. For the feedwater salinity of 35 g/kg, the limitation of specific water production increases as the recovery ratio (rr) decreases for the system that operates at ambient pressure (P_0). For the range of concentration ratio (C) is (a) 1–5 and (b) 10–50, a higher concentration ratio or solar irradiance intensity allows the solar desalination system to have a higher specific water production potential.

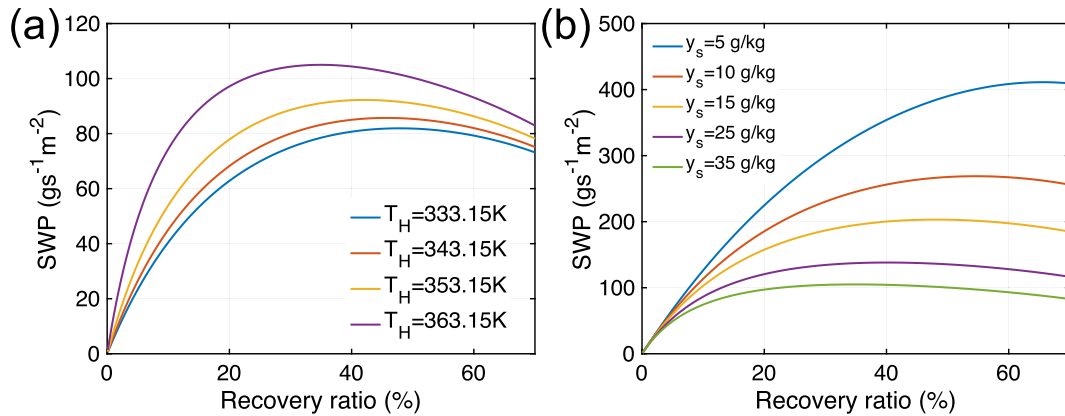


Fig. 6. (a) When the recovery rate of flow work $r_f = 0$, and the salinity of incoming water is 35 g/kg, higher evaporator temperature (T_H) can achieve larger specific water production and the corresponding optimal recovery ratio decreases. (b) When the evaporator temperature keeps at 363.15 K, the lower salinity of incoming water makes the solar thermal desalination system performs the better, and the corresponding optimal recovery ratio increases.

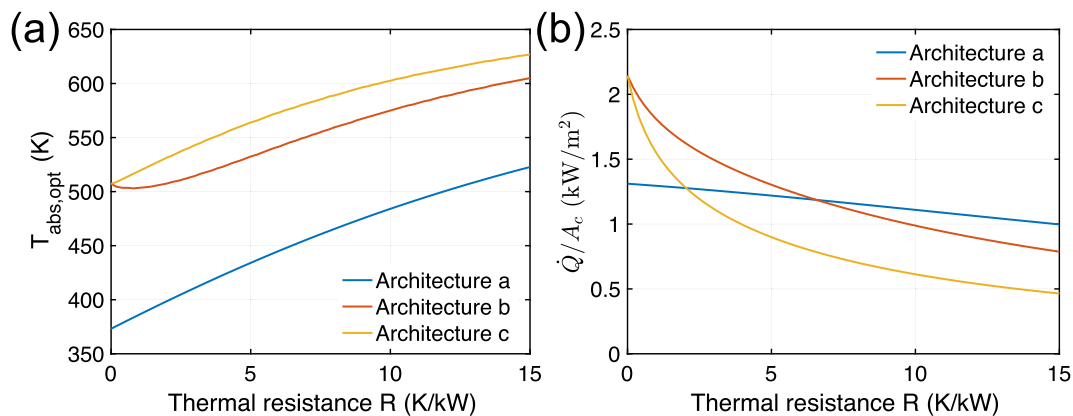


Fig. 7. (a) The overall trend of optimal absorber temperature ($T_{abs,opt}$) under irreversible condition increases with thermal resistance (R) at evaporator temperature $T_H = 373.15$ K. While there is a small drop of optimal temperature for heating architecture **b** when the thermal resistance is relatively small. The optimal temperature of architecture **c** is the highest, while that of architecture **a** is the lowest. (b) The heating architecture **b** can supply more heat at relatively low thermal resistance. Architecture **a** has a better performance when the thermal resistance larger than 6.5 K/kW.

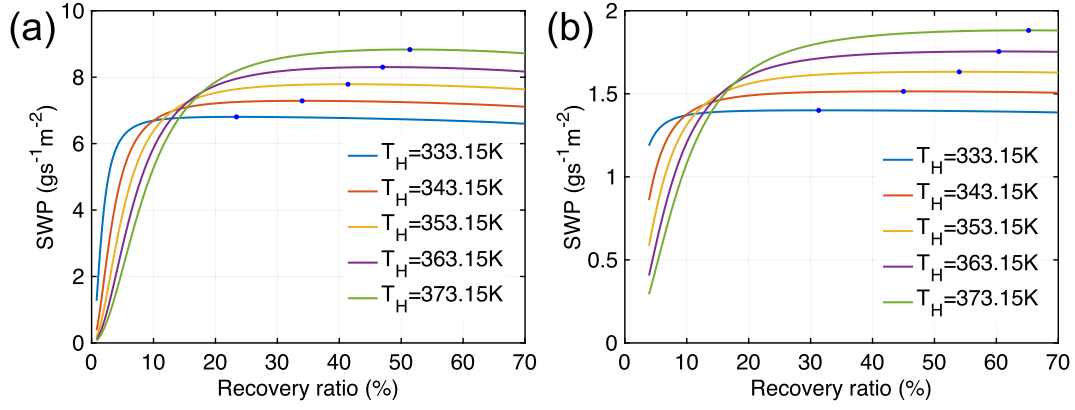


Fig. 8. For the irreversible solar thermal desalination system with heating architecture **b**, each of the thermal resistance of (a) $R = 0.001$ K/kW, (b) $R = 0.005$ K/kW, inlet temperature of heater 1 (H1) $T_L = 323.15$ K, inlet saline water salinity $y_s = 35$ g/kg, and the recovery rate of flow work $r_f = 100\%$, the optimal recovery ratio increases as evaporator temperature (T_H) increases. When evaporator temperature is relatively smaller, specific water production (SWP) can reach stable value faster with the increase of recovery ratio. Before reaching the stable value, the lower the evaporator temperature, the higher the SWP. However, SWP is larger with higher evaporator temperatures after it reaches a stable value.

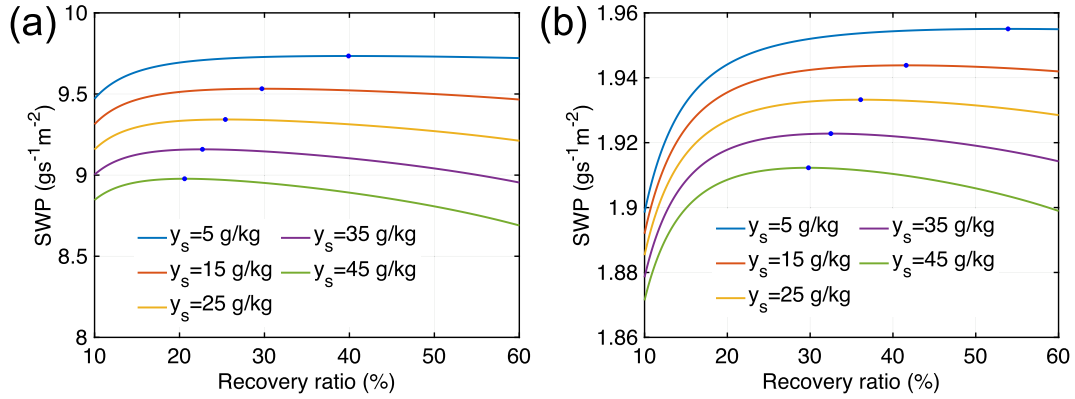


Fig. 9. For the irreversible solar thermal desalination system with heating architecture **b**, each of the thermal resistance of (a) $R = 0.001$ K/kW, (b) $R = 0.005$ K/kW, evaporator temperature $T_H = 373.15$ K and inlet temperature of heater 1 (H1) $T_L = 363.15$ K, and the recovery rate of flow work $r_f = 100\%$, the lower inlet saline water salinity (y_s) can reach the higher maximum specific water production (SWP) and the corresponding recovery ratio.

$$\dot{Q}_u - \dot{Q}_4 = \dot{Q}_3 - \dot{Q}_5 \quad (21)$$

$$\frac{\dot{Q}_3}{\dot{Q}_5} = \frac{T_H + \dot{Q}_3 \cdot R}{T_0 - \dot{Q}_5 \cdot R} \quad (22)$$

3.2.2. Distillation system

The change in flow exergy per unit mass of produced water for each component inlet and outlet in the distillation system under reversible conditions is:

$$w = \frac{\dot{W}}{\dot{m}_p} = \frac{\dot{m}_{in} \psi_{in}(T_{in}, y_{in}, P_{in}) - \dot{m}_{out} \psi_{out}(T_{out}, y_{out}, P_{out})}{\dot{m}_p} \quad (23)$$

where ψ is the specific flow exergy. It can be calculated by the change of specific Gibbs free energy (g) with respect to the environmental state. The condenser releases heat at an operating temperature (T_C). According to the specific maximum work ($w_{HE,con}$) of the Carnot engine under reversible conditions, the heat release rate at the condenser is

$$\dot{Q}_{con} = \dot{m}_p \frac{w_{HE,con}}{1 - \frac{T_0}{T_C}} \quad (24)$$

The endo-reversible heat engine model consider that irreversibilities and thus the heat release rate from the heat engine to the environment can be

evaluated by:

$$\frac{\dot{Q}_{con}}{\dot{Q}_{con,0}} = \frac{T_C - \dot{Q}_{con} \cdot R}{T_0 + \dot{Q}_{con,0} \cdot R} \quad (25)$$

Therefore, the work output of the heat engine per unit mass of fresh-water production under the specific irreversibility is:

$$\frac{w_{HE,con,irr}}{\dot{m}_p} = \frac{\dot{Q}_{con} - \dot{Q}_{con,0}}{\dot{m}_p} \quad (26)$$

Summing up the work that each component needs or does after considering the thermal resistance and possible flow work (w_f) is the actual minimum work of separation by the system under an irreversible state ($w_{sep,irr}$). Since the solar collector supplies heat to the evaporator with the operating temperature of T_H , the minimum heat of separation is:

$$q_{sep,irr} = \frac{w_{sep,irr}}{1 - \frac{T_0}{T_H}} \quad (27)$$

4. Results and discussion

Solar-thermal desalination is currently plagued with low efficiencies and high levelized cost of water because of the energy quality mismatch

between solar collectors (high) and desalination systems (low). Here, we investigate three different integration strategies, which may enable integration of high energy solar collectors with desalination systems (Fig. 2). Fundamental performance limits of ideal (Carnot) systems are discussed and compared with non-ideal systems (Fig. 3). We also explore the impact of technical and operational parameters (such as thermal resistance, absorber temperature, feedwater salinity) on the performance. The results can provide generalized guidelines for future plant designs and motivates hybridization approaches (heat pump-based, and cogeneration, etc.) that can improve the performance of solar-desalination systems.

4.1. Reversible scenario

During reversible operation (i.e., ideal), the heat transfer rate for architecture **b** and **c** are the same, and will have higher heat transfer rates than the direct heating architecture **a** (Fig. 2a-c) for finite temperature difference heat transfer (Supporting Information S2). Thus, all subsequent reversible analysis of performance limitation, is relevant to architectures **b** and **c** [53,54]. The concentration ratio is an important design variable because it is directly relevant to the amount of harvested energy (Eq. (4)), thereby affecting the water production performance. The larger the concentration ratio, the higher the optimal surface temperature ($T_{abs,opt}$) and maximum normalized heat (\dot{Q}_{max}/A_c) (Fig. 4). The rate at which the optimal surface temperature and maximum normalized heat supply increases, decreases with concentration ratio. While the quality of the collected thermal energy is higher at elevated temperatures, excessive heat dissipation is also possible. The latter can reduce the growth rate of maximum heat supply. When the concentration ratio is less than 100, the optimal temperature and maximum normalized heat increases at a decreasing rate. Prior work has also seen similar results, suggesting that the operating temperature and maximum power production of a CSP system is directly a function of the receiver irradiance [34].

To understand performance limitations with solar desalination systems we assumed the highest possible solar irradiance intensity and compared it to $I_s = 1000 \text{ W/m}^2$. The latter intensity is a common solar illumination intensity in laboratory experiments (Fig. 4 and 5). Solar irradiance intensity in an actual system will vary by geographic location. When the concentration ratio is 10, the optimal absorber temperature ($T_{abs,opt}$) is 507 K and the maximum normalized heat supply to the evaporator (\dot{Q}_{max}/A_c) is 2.14 kW/m^2 (Fig. 4). These two parameters decrease to 481 K and 1.4 kW/m^2 at the lower irradiance level ($1000 = \text{W/m}^2$), while the overall trends with concentration ratio (C) remain the same. Therefore, based on Eq. (1), the maximum specific water production (SWP) will also decrease proportionally due to the reduction of the normalized heat supply (Fig. 5). For a distillation system that operates at ambient pressure (P_0), the maximum SWP increases as recover ratio (rr) decreases (Fig. 5a). Systems with low recovery ratios require less energy for separation according to Eq. (9). Higher concentration ratios and solar insolation levels result in greater maximum normalized heat supply (\dot{Q}_{max}/A_c) and therefore higher specific water production (Fig. 5b). For a system with a concentration ratio of 10, the maximum specific water production is $166.3 \text{ gs}^{-1}\text{m}^{-2}$ as the recovery ratio approaches zero (Fig. 5b).

If we consider a distillation system that operates below ambient pressure (via considering flow work), the optimal recovery ratio is no longer zero. The desalination system will require an infinitely large flow work to achieve flow rates below atmospheric pressure as the recovery ratio approaches zero. The optimal recovery ratio for the case that flow work cannot be fully recovered ($r_f < 100\%$) is relevant to evaporator temperature (Fig. 6a) and salinity of incoming water (Fig. 6b). Under various evaporator temperatures (T_H) in terms of operating pressure (P), different optimal recovery ratios maximize the specific water production (SWP). Furthermore, the optimal recovery ratio decreases as the

evaporator temperature (T_H) increases. For the same recovery ratio, the SWP increases with the evaporator temperature in terms of operating pressure (P). This is inconsistent with the actual thermal desalination systems (e.g., multi-stage distillation system), that perform better when operating below the atmospheric pressure. The ideal analysis assumes that the evaporating surface and condensation surface are infinitely large and close to each other and that the brine does not contain dissolved gases. Hence, the mass transfer resistances are negligible. We will further discuss which of the thermal resistance between the heat exchange surfaces and the flow work due to pressure difference has a greater impact on the system's performance in the irreversible scenario subsection.

When the evaporator temperature (363.15 K) and the recovery ratio (rr) is held constant, we observe an increase in the specific water production (SWP) as the salinity of the feedwater decreases. This is due to a decrease in the minimum separation work necessary to treat low salinity solutions[40]. When the salinity decreases from 35 g/kg to 15 g/kg, the maximum specific water production increases from $105.0 \text{ gs}^{-1}\text{m}^{-2}$ (Fig. 6b) to $203.1 \text{ gs}^{-1}\text{m}^{-2}$, and the optimal recovery ratio rises from 34.9% to 48.1%. The optimal recovery ratio for the maximum specific water production decreases as the salinity increases. When the recovery ratio is close to zero, the influence of the incoming water salinity (y_s) on SWP is less significant.

4.2. Irreversible scenario

During irreversible operating conditions, the optimal surface temperature of the solar collector ($T_{abs,opt}$) will be lowest for heating architecture **a** and greatest for heating architecture **c**. As the thermal resistance increases, we observe an increase in the optimized absorber temperature for each configuration (Fig. 7) and a decrease in the optimum heat transfer rate (Fig. 7b) in comparison to the ideal case where concentration ratio is 10 (Fig. 4). However, when the thermal resistance is small, architecture **b** demonstrates a slight decrease in the optimal absorber temperature. The increase in thermal resistance negates the absorber temperature's impact on the system efficiency. Therefore, at low thermal resistances, there may be some benefit to lowering the solar collector temperature (architecture **b**) to reduce the heat loss and maximize heat supply. Due to the exergy loss caused by heat transfer with finite temperature difference, the normalized heat supply of heating configuration **a** is the lowest when the thermal resistance is relatively small (Fig. 7b). When the thermal resistance is less than the critical point ($R = 6.5 \text{ K/kW}$), the heating configuration **b** is the optimum. However, as the thermal resistance increases, the advantages brought by the heat engine and heat pump become insignificant, and direct heating becomes advantageous. The solar collector system design (i.e., concentration ratio, absorber temperature, and heating configuration) impacts the thermal resistance and the operating temperature of the desalination system. Concentrating technologies raise the ideal heat supply rate for the non-direct heating configurations (Fig. 4). However, when irreversibilities are included, the heat transfer rate is more sensitive to the thermal resistance (Eq. (14)). Therefore, architecture **b** with a high concentration ratio solar collector is more applicable for plants that can accommodate large heat-exchangers (large scale systems). Otherwise, a direct heating strategy (architecture **a**) with a concentration ratio that allows the absorber temperature to match the evaporator temperature is preferable.

Irreversibilities in both the solar collector and the distillation system seriously damage the specific water production (SWP) and increases the optimal recovery ratio (Fig. 8a and b). Therefore, it is crucial to reduce the irreversibilities by increasing the area and heat transfer coefficient of the heat exchanger without increasing system cost. The distillation process is more sensitive to the thermal resistance (R) than the solar collector heating architecture when the concentration ratio is 10 (Fig. 7b) because the energy demand to overcome the latent heat of vaporization is two orders of magnitude higher than the minimum heat

of separation. As the thermal resistance increases from 0.001 K/kW to 0.005 K/kW for heating configuration **b**, a decrease in the optimal SWP is observed from $8.8 \text{ gs}^{-1}\text{m}^{-2}$ ($rr = 51.4\%$) to $1.9 \text{ gs}^{-1}\text{m}^{-2}$ ($rr = 65.2\%$). Both irreversible cases demonstrate significantly lower SWP when compared to the ideal scenario with flow work ($81.9 \text{ gs}^{-1}\text{m}^{-2}$ at $T_H = 333.15 \text{ K}$). Therefore, when the recovery ratio (rr) is greater than 0, the negative impact of flow work on SWP (Fig. 6a) is much smaller than the thermal resistance in the energy recovery process. It is worth sacrificing energy consumption for flow work in order to decrease the mass transfer thermal resistance between the evaporating and condensing surfaces and for greater water production.

Neglecting the impact of flow work (by considering $r_f = 100\%$), the specific water production (SWP) approaches 0 when the recovery ratio (rr) is low (Fig. 8a and b). It is a result of the large heat exchange in heater 1 (H1) and chiller 2 (C2) due to the high mass flow rate and inefficient energy recovery due to system irreversibilities. The effect is more pronounced when the evaporator temperature (T_H) is relatively high since there is a greater energy requirement for the preheating process. The SWP increases at higher recovery ratios because there is less exergy destruction between the evaporator and solar collector, and the energy released in condenser has a higher exergy $\dot{Q}_{con}(1 - \frac{T_0}{T_c})$ for reuse. The thermal resistance has less of an impact on the energy recovery system for the high-temperature system but does impact the energy recovery in the low-temperature system. When the recovery ratio is increased to a critical value (e.g., $\sim 9\%$ for $T_H = 333.15 \text{ K}$), the preheating process has negligible effect on the system performance and the SWP is independent of the recovery ratio. Thus, higher evaporator operating temperatures (T_H) are beneficial for system performance. This trend is similar to previously reported studies that show that higher top brine temperatures enable a higher freshwater production rate [65]. Overall, the SWP shows independent of the evaporator operating temperature at high recovery ratios (Fig. 8a and b). Thus, thermal desalination technologies are suitable for high-recovery water treatment. However, when the recovery ratio cannot be engineered, the adoption of a low-temperature distillation process ($P < P_0$) may improve SWP by avoiding unnecessary exergy destruction during the preheating process.

The salinity of the feedwater plays a significant role on the specific water production (SWP) under reversible conditions (Fig. 6b), but has little impact on the specific water consumption in systems with irreversibilities (Fig. 9a and b). Experimental results on a membrane distillation system show a similar trend where the SWP is not dependent on the salinity of the feedwater [66]. The optimal recovery ratio of a system with irreversibilities is affected by energy recovery in the preheating stage and heat rejection process as well as changes in the feedwater chemical potential. When the recovery ratio (rr) is low, the SWP suffers from a large mass flow rate and the salinity has minimal impact on the SWP. As the recovery ratio increases, the change in Gibbs free energy due to salinity changes dominates and results in a decrease in SWP with recovery ratio (Fig. 9b). At low feedwater salinities the SWP is independent of the recovery ratio (Eq. 8). Therefore, when the salinity decreases, both the maximum SWP and optimal rr increase. The maximum specific water production will increase from $9.2 \text{ gs}^{-1}\text{m}^{-2}$ to $9.7 \text{ gs}^{-1}\text{m}^{-2}$, and the optimal recovery ratio will increase from 22.7% to 39.9% if the salinity is decreased from 35 g/kg to 5 g/kg ($R = 0.001 \text{ K/kW}$). When the incoming water salinity and the irreversible degree of the designed desalination system are higher, the adjustment in recovery ratio (rr) by modifying the inlet mass flow rate (\dot{m}_i) will enhance the performance relatively more obvious.

5. Conclusion and outlook

Solar thermal desalination technologies are ideal for geographic regions that experience water scarcity challenges and have an abundance of solar energy [1,17]. However, it is currently energy inefficient to couple solar with desalination and nearly 99% of all desalination plants

utilize CO₂ emitting fossil fuels. Herein, we evaluate three different heating modes which may enable the coupling of solar collectors with thermal desalination systems. The generalized models developed are suitable for a technology agnostic analysis of solar thermal desalination systems and thus is a valuable reference for future solar water desalination designers.

Architecture **a** is a direct heating strategy and architectures **b** and **c** utilize an energy recovery method (e.g., using Carnot heat engines and Carnot heat pumps) to avoid the exergy destruction caused by finite temperature difference heat transfer. A solar desalination system with a concentration ratio of 10 has the performance limit of specific water production of $\sim 166 \text{ g s}^{-1}\text{m}^{-2}$ as the recovery ratio approaches zero. When the thermal desalination system operates below atmospheric pressure, its performance limit drops due to the flow work (e.g., when the evaporator temperature drops to 363.15K, the maximum SWP is $105.0 \text{ gs}^{-1}\text{m}^{-2}$ at the optimal recovery ratio of 34.9%). In order to understand the role irreversibilities have on system performance, we implement and evaluate endo-reversible heat engines and pumps. Highly irreversible solar thermal desalination systems benefit from direct heating strategies (architecture **a**) and systems with low irreversibilities ($R < 6.5 \text{ K/kW}$ for $C = 10$) benefit from cascading heat transfer approach (architecture **b**). Neither scenarios benefit from a lumped approach (architecture **c**). High-concentration solar collectors are more susceptible to thermal resistance due to their higher heat transfer rate. Therefore, systems based on high-concentration ratio technologies are more suitable for large-scale systems that can economically accommodate large area heat exchangers.

Actual systems (e.g., irreversible systems) should avoid an extremely low recovery ratio because it will result in high mass flow rates in the distillation system. However, lowering the evaporator temperature may benefit overall system performance in these cases. The thermal resistance of the heat exchange surface ($R = 0.001 \text{ k/kW}$) can reduce SWP considerably as results show a decrease from the ideal performance limit of $\sim 166 \text{ gs}^{-1}\text{m}^{-2}$ ($rr = 0$) to $8.8 \text{ gs}^{-1}\text{m}^{-2}$ ($rr = 51.4\%$). The influence of thermal resistance on SWP is more significant than factors such as flow work and incoming water salinity. Therefore, the design should prioritize increasing the area A_e and the heat transfer coefficient U of the heat exchange surfaces. Optimization of sub-system performance parameters is going to be paramount for next-generation desalination systems based on renewable energy.

Declaration of Competing Interest

The authors declare that they have no known competing financial interests or personal relationships that could have appeared to influence the work reported in this paper.

Acknowledgment

K.B.H and Y.Z. acknowledge support by the National Science Foundation under Grant No. 1706956 and M.C.H. and R.C.G. acknowledge support from National Science Foundation under No. 1706290. R.C.G. acknowledges support from the National Agency for Research and Development (ANID)/Scholarship Program/ DOCTORADO BECAS CHILE/2018-72190312.

Appendix A. Supplementary material

Supplementary data associated with this article can be found, in the online version, at <https://doi.org/10.1016/j.applthermaleng.2020.116292>.

References

- [1] Y. Zheng, K.B. Hatzell, Technoeconomic analysis of solar thermal desalination, *Desalination* 474 (2020) 114168.

- [2] H.-J. Joo, H.-Y. Kwak, Performance evaluation of multi-effect distiller for optimized solar thermal desalination, *Appl. Therm. Eng.* 61 (2) (2013) 491–499.
- [3] Y.H. Zurigat, M.K. Abu-Arabi, Modelling and performance analysis of a regenerative solar desalination unit, *Appl. Therm. Eng.* 24 (7) (2004) 1061–1072.
- [4] J. Zhang, K.B. Hatzell, M.C. Hatzell, A combined heat-and power-driven membrane capacitive deionization system, *Environ. Sci. Technol. Lett.* 4 (11) (2017) 470–474.
- [5] Rodrigo A. Caceres Gonzalez, Yanjie Zheng, Kelsey B. Hatzell, Marta C. Hatzell, Optimizing a cogeneration sCO₂ CSP–MED plant using neural networks, *ACS ES & T Eng.* <https://doi.org/10.1021/accestengg.0c00132>.
- [6] A.M. Bilton, R. Wiesman, A. Arif, S.M. Zubair, S. Dubowsky, On the feasibility of community-scale photovoltaic-powered reverse osmosis desalination systems for remote locations, *Renew. Energy* 36 (12) (2011) 3246–3256.
- [7] A. Ghermandi, R. Messale, Solar-driven desalination with reverse osmosis: the state of the art, *Desalination Water Treatment* 7 (1–3) (2009) 285–296.
- [8] Y. Pang, J. Zhang, R. Ma, Z. Qu, E. Lee, T. Luo, Solar-thermal water evaporation: A review, *ACS Energy Lett.*
- [9] I.S. Al-Mutaz, I. Wazeer, Comparative performance evaluation of conventional multi-effect evaporation desalination processes, *Appl. Therm. Eng.* 73 (1) (2014) 1194–1203.
- [10] S. Islam, I. Dincer, B.S. Yilbas, Development of a novel solar-based integrated system for desalination with heat recovery, *Appl. Therm. Eng.* 129 (2018) 1618–1633.
- [11] M.B. Dixit, D. Moreno, X. Xiao, M.C. Hatzell, K.B. Hatzell, Mapping charge percolation in flowable electrodes used in capacitive deionization, *ACS Mater. Lett.* 1 (1) (2019) 71–76.
- [12] K.H. Mistry, R.K. McGovern, G.P. Thiel, E.K. Summers, S.M. Zubair, J.H. Lienhard, Entropy generation analysis of desalination technologies, *Entropy* 13 (10) (2011) 1829–1864.
- [13] H. Zheng, Solar energy desalination technology, Elsevier, 2017.
- [14] M.C. Hatzell, K.B. Hatzell, Blue refrigeration: Capacitive de-ionization for brackish water treatment, *Journal of Electrochemical Energy Conversion and Storage* 15 (1).
- [15] D. Moreno, Y. Bootwala, W.-Y. Tsai, Q. Gao, F. Shen, N. Balke, K.B. Hatzell, M. C. Hatzell, In situ electrochemical dilatometry of phosphate anion electroadsorption, *Environ. Sci. Technol. Lett.* 5 (12) (2018) 745–749.
- [16] H. Arafat, Desalination Sustainability: A Technical, Socioeconomic, and Environmental Approach, Elsevier, 2017.
- [17] A. Pugsley, A. Zacharopoulos, J.D. Mondol, M. Smyth, Global applicability of solar desalination, *Renew. Energy* 88 (2016) 200–219.
- [18] A. Al-Karaghoul, L.L. Kazmerski, Energy consumption and water production cost of conventional and renewable-energy-powered desalination processes, *Renew. Sustain. Energy Rev.* 24 (2013) 343–356.
- [19] K. Mohammadi, M. Saghaffar, K. Ellingwood, K. Powell, Hybrid concentrated solar power (csp)-desalination systems: A review, *Desalination* 468 (2019) 114083.
- [20] P. Palenzuela, G. Zaragoza, D.C. Alarcón-Padilla, E. Guillén, M. Ibarra, J. Blanco, Assessment of different configurations for combined parabolic-trough (pt) solar power and desalination plants in arid regions, *Energy* 36 (8) (2011) 4950–4958.
- [21] P. Palenzuela, G. Zaragoza, D. Alarcón, J. Blanco, Simulation and evaluation of the coupling of desalination units to parabolic-trough solar power plants in the mediterranean region, *Desalination* 281 (2011) 379–387.
- [22] J. Blanco, P. Palenzuela, D. Alarcón-Padilla, G. Zaragoza, M. Ibarra, Preliminary thermo-economic analysis of combined parabolic trough solar power and desalination plant in port safaga (egypt), *Desalination Water Treatment* 51 (7–9) (2013) 1887–1899.
- [23] G. Iaquaniello, A. Salladini, A. Mari, A. Mabrouk, H. Fath, Concentrating solar power (csp) system integrated with med-ro hybrid desalination, *Desalination* 336 (2014) 121–128.
- [24] Y. Xue, X. Du, Z. Ge, L. Yang, Study on multi-effect distillation of seawater with low-grade heat utilization of thermal power generating unit, *Appl. Therm. Eng.* 141 (2018) 589–599.
- [25] M.T. Ali, H.E. Fath, P.R. Armstrong, A comprehensive techno-economic review of indirect solar desalination, *Renew. Sustain. Energy Rev.* 15 (8) (2011) 4187–4199.
- [26] S. Avlonitis, K. Kouroumbas, N. Vlachakis, Energy consumption and membrane replacement cost for seawater ro desalination plants, *Desalination* 157 (1) (2003) 151–158.
- [27] I.B. Askari, M. Ameri, Techno economic feasibility analysis of linear fresnel solar field as thermal source of the med/tvc desalination system, *Desalination* 394 (2016) 1–17.
- [28] M.A. Sharaf, Thermo-economic comparisons of different types of solar desalination processes, *Journal of solar energy engineering* 134 (3).
- [29] B.F. Tchanche, G. Papadakis, G. Lambrinos, A. Frangoudakis, Fluid selection for a low-temperature solar organic rankine cycle, *Appl. Therm. Eng.* 29 (11–12) (2009) 2468–2476.
- [30] J.C. Bruno, J. Lopez-Villada, E. Letelier, S. Romera, A. Coronas, Modelling and optimisation of solar organic rankine cycle engines for reverse osmosis desalination, *Appl. Therm. Eng.* 28 (17–18) (2008) 2212–2226.
- [31] P. Palenzuela, B. Ortega-Delgado, D.-C. Alarcón-Padilla, Comparative assessment of the annual electricity and water production by concentrating solar power and desalination plants: A case study, *Appl. Therm. Eng.* 177 (2020) 115485.
- [32] M.J. Aberue, E. Baniyasi, M. Ziaei-Rad, Performance analysis of an integrated solar based thermo-electric and desalination system, *Appl. Therm. Eng.* 110 (2017) 399–411.
- [33] H. Zheng, X. Yu, Y. Su, S. Riffat, J. Xiong, Thermodynamic analysis of an idealised solar tower thermal power plant, *Appl. Therm. Eng.* 81 (2015) 271–278.
- [34] R.K. McGovern, W.J. Smith, Optimal concentration and temperatures of solar thermal power plants, *Energy Convers. Manage.* 60 (2012) 226–232.
- [35] K.H. Kim, C.H. Han, A review on solar collector and solar organic rankine cycle (orc) systems, *J. Autom. Control Eng.* 3 (1) (2015) 66–73.
- [36] G. Qiu, J. Sun, L. Nie, Y. Ma, W. Cai, C. Shen, Theoretical study on heat transfer characteristics of a finned tube used in the collector/evaporator under solar radiation, *Appl. Therm. Eng.* 165 (2020) 114564.
- [37] R. Moss, G. Shire, P. Henshall, P.C. Eames, F. Arya, T. Hyde, Design and fabrication of a hydroformed absorber for an evacuated flat plate solar collector, *Appl. Therm. Eng.* 138 (2018) 456–464.
- [38] I.H. Njoku, C.O. Oko, J.C. Ofodu, O.E. Diemuodeke, Optimal thermal power plant selection for a tropical region using multi-criteria decision analysis, *Appl. Therm. Eng.* 179 (2020) 115706.
- [39] L. Xu, J. Yuan, Thermodynamic properties calculation of the flue gas based on its composition estimation for coal-fired power plants, *Appl. Therm. Eng.* 90 (2015) 366–375.
- [40] Y. Cerci, The minimum work requirement for distillation processes, *Exergy, An Int. J.* 2 (1) (2002) 15–23.
- [41] D. Brogioli, F. La Mantia, N.Y. Yip, Thermodynamic analysis and energy efficiency of thermal desalination processes, *Desalination* 428 (2018) 29–39.
- [42] D. Zhao, S. Deng, Y. Shao, L. Zhao, P. Lu, W. Su, A new energy analysis model of seawater desalination based on thermodynamics, *Energy Proc.* 158 (2019) 5472–5478.
- [43] L. Chen, L. Shu, Y. Ge, F. Sun, Minimum energy requirement of an endoreversible desalination system of sea water, *Int. J. Energy Environ.* 6 (4) (2015) 331.
- [44] S. Sieniutycz, J. Jezowski, Energy optimization in process systems and fuel cells, Elsevier, 2018.
- [45] D. Moreno, M.C. Hatzell, Efficiency of carnot and conventional capacitive deionization cycles, *J. Phys. Chem. C* 122 (39) (2018) 22480–22486.
- [46] F.E. Ahmed, R. Hashaikh, N. Hilal, Solar powered desalination–technology, energy and future outlook, *Desalination* 453 (2019) 54–76.
- [47] Z. Chang, H. Zheng, Y. Yang, Y. Su, Z. Duan, Experimental investigation of a novel multi-effect solar desalination system based on humidification–dehumidification process, *Renew. Energy* 69 (2014) 253–259.
- [48] C. Li, Y. Goswami, E. Stefanakos, Solar assisted sea water desalination: A review, *Renew. Sustain. Energy Rev.* 19 (2013) 136–163.
- [49] H. Zhang, J. Baeyens, J. Degève, G. Caceres, Concentrated solar power plants: Review and design methodology, *Renew. Sustain. Energy Rev.* 22 (2013) 466–481.
- [50] M.W. Shahzad, M. Burhan, L. Ang, K.C. Ng, Energy-water-environment nexus underpinning future desalination sustainability, *Desalination* 413 (2017) 52–64.
- [51] Z.M. Amin, M.N.A. Hawlader, Analysis of solar desalination system using heat pump, *Renew. Energy* 74 (2015) 116–123.
- [52] A. Rabl, Active solar collectors and their applications, Oxford University Press on Demand, 1985.
- [53] H. Zheng, T. Tao, J. Dai, H. Kang, Light tracing analysis of a new kind of trough solar concentrator, *Energy Convers. Manage.* 52 (6) (2011) 2373–2377.
- [54] C. Feng, H. Zheng, R. Wang, X. Ma, Performance investigation of a concentrating photovoltaic/thermal system with transmissive fresnel solar concentrator, *Energy Convers. Manage.* 111 (2016) 401–408.
- [55] A. Deshmukh, C. Boo, V. Karanikola, S. Lin, A.P. Straub, T. Tong, D.M. Warsinger, M. Elimelech, Membrane distillation at the water-energy nexus: limits, opportunities, and challenges, *Energy Environ. Sci.* 11 (5) (2018) 1177–1196.
- [56] M. Elimelech, W.A. Phillip, The future of seawater desalination: energy, technology, and the environment, *Science* 333 (6043) (2011) 712–717.
- [57] D. Warsinger, K. Mistry, K. Nayar, H. Chung, V. Lienhard, et al., Entropy generation of desalination powered by variable temperature waste heat, *Entropy* 17 (11) (2015) 7530–7566.
- [58] K.G. Nayar, M.H. Sharqawy, L.D. Banchik, et al., Thermophysical properties of seawater: a review and new correlations that include pressure dependence, *Desalination* 390 (2016) 1–24.
- [59] W. Wagner, A. Pruß, The iapws formulation 1995 for the thermodynamic properties of ordinary water substance for general and scientific use, *J. Phys. Chem. Reference Data* 31 (2) (2002) 387–535.
- [60] M.H. Sharqawy, J.H. Lienhard, S.M. Zubair, Thermophysical properties of seawater: a review of existing correlations and data, *Desalination Water Treatment* 16 (1–3) (2010) 354–380.
- [61] B.M. Fabuss, A. Korosi, Boiling point elevations of sea-water and its concentrates, *J. Chem. Eng. Data* 11 (4) (1966) 606–609.
- [62] L.A. Bromley, D. Singh, P. Ray, S. Sridhar, S.M. Read, Thermodynamic properties of sea salt solutions, *AIChE J.* 20 (2) (1974) 326–335.
- [63] A.Z. Sahin, Finite-time thermodynamic analysis of a solar driven heat engine, *Exergy, An Int. J.* 1 (2) (2001) 122–126.
- [64] Y. Zheng, Y. Zhao, S. Liang, H. Zheng, Thermo-economic optimization of an idealized solar tower power plant combined with med system, *Entropy* 20 (11) (2018) 822.
- [65] C. Hanshik, H. Jeong, K.-W. Jeong, S.-H. Choi, Improved productivity of the msf (multi-stage flashing) desalination plant by increasing the tbt (top brine temperature), *Energy* 107 (2016) 683–692.
- [66] S. Adham, A. Hussain, J.M. Matar, R. Dores, A. Janson, Application of membrane distillation for desalting brines from thermal desalination plants, *Desalination* 314 (2013) 101–108.